Solar Phys (2010) 264: 165–188
DOI 10.1007/s11207-010-9554-z

High-Speed Solar Wind Streams during 1996 – 2007: Sources, Statistical Distribution, and Plasma/Field Properties

V. Gupta · Badruddin

Received: 18 May 2009 / Accepted: 4 April 2010 / Published online: 5 May 2010

Abstract We present a catalog of high-speed streams, along with their solar sources for solar cycle 23. We study their distribution during different years and different phases of solar cycle after classifying them into different groups based on their source(s), duration, and speed. We also study the average plasma/field properties of streams after dividing them into suitable groups on the basis of their source(s), duration and speed. It is expected that the catalog and statistical results presented in this work will further stimulate the space weather and solar-terrestrial studies involving high-speed streams.

Keywords High speed stream · Solar wind · Solar-terrestrial physics · Space weather

1. Introduction

Research in the area of solar-terrestrial and heliospheric physics has grown remarkably in the last few decades, particularly after the availability of useful solar/interplanetary plasma and field data from both space and ground-based observations. Continuous flow of the slow solar wind of speed $\approx 250-400$ km s^{-1} (Parker, 1959; Gold, 1959) is often superposed by faster streams, which cause shock fronts by stream-stream interactions. These fast streams are characterized by a typical speed of $400-800$ km s^{-1}. Coronal holes (CH) are long-lived regions of low density and temperature, and occur in open and diverging unipolar field regions. As the sun rotates, coronal holes pass across the Sun – Earth line and the Earth encounters streams of high-speed solar wind for periods lasting several days. As the high-speed streams are emitted from the Sun, they catch up with the previously emitted solar wind and form a compressed interface in the interplanetary medium called a corotating interaction region (see, *e.g.*, Morley, Rouillard, and Freeman (2009) and references therein). Then, there are

Electronic supplementary material The online version of this article (doi:10.1007/s11207-010-9554-z) contains supplementary material, which is available to authorized users.

V. Gupta · Badruddin (✉)
Department of Physics, Aligarh Muslim University, Aligarh 202 002, India
e-mail: badr.physamu@gmail.com

ejections from the Sun, called coronal mass ejections (CMEs), some of them fast enough to drive a shock. A small part of all the CMEs head towards the Earth; these CMEs get fairly modified by the time they reach the Earth orbit (1 AU) considerably influencing the plasma and field properties of the solar wind (Manoharan *et al.*, 2004). The interplanetary counterpart of CMEs (ICMEs) as seen near 1 AU are of dimensions $\approx 0.2 - 0.3$ AU and generally have a shock front followed by ejecta, with complicated magnetic field configurations. A subset of ICMEs are magnetic clouds, characterized by high magnetic fields, low proton temperature, low plasma beta (ratio between thermal and magnetic pressure), and a smooth rotation of the magnetic components (*e.g.*, Burlaga *et al.*, 1981; Klein and Burlaga, 1982; Lepping, Jones, and Burlaga, 1990; Burlaga, 1991; Mulligan and Russell, 2001; Gosling, 1996; Kane, 2007).

Till early 1990s the solar flares acquired the central position in most of the solar-terrestrial phenomena (*e.g.*, Rao, 1972; Agrawal *et al.*, 1974; Venkatesan, Shukla, and Agrawal, 1982; Mikhailutsa and Gnevyshev, 1985; Iucci *et al.*, 1979, 1984; Filisetti *et al.*, 1988; Venkatesan and Badruddin, 1990). However, after the publication of Gosling (1993) paper and availability of good quality coronagraph data, the CMEs, instead of the solar flares, acquired central importance in producing major events in near-Earth space environment (Cane, 2000; Crooker, 2000; Gopalswamy, 2006; Borovsky and Denton, 2006; Schwenn, 2006; Pulkkinen, 2007).

In the past, the high-speed solar-wind streams were attributed to solar flares and CH (*e.g.*, Lindblad and Lundstedt, 1981, 1983; Lindblad, Lundstedt, and Larsson, 1989; Mavromichalaki, Vassilaki, and Marmatsouri, 1988; Mavromichalaki and Vassilaki, 1998). However, after the advent of coronagraph and space-based near-Earth observations of the solar-wind, high-speed streams in the solar-wind plasma are recognized as those ejected from solar active regions during the time of CMEs and those coming from coronal holes (Gosling, 1996; Sabbah, 2000; Jian *et al.*, 2006a, 2006b; Kane, 2007).

Solar-terrestrial effects of two distinct types, one due to solar-wind streams associated with CMEs and other due to CH are being observed and studied for several decades. For example, corotating and transient decreases in cosmic-ray intensity (*e.g.*, Cane, 2000; Sabbah, 2000; Singh and Badruddin, 2007a, 2007b), CME- and CIR-driven geomagnetic storms (*e.g.*, Badruddin, 1998; Richardson *et al.*, 2006; Alves, Echer, and Gonzalez, 2006; Zhang *et al.*, 2007; Echer *et al.*, 2008; Turner *et al.*, 2009) have been the subject of great interest. However, in addition to transient changes in cosmic-ray intensity and geomagnetic activity, corotating variations in cosmic-ray intensity and recurrent geomagnetic activity, long-lived cosmic-ray depressions, 'cosmic-ray storms' (Kane, 1977; Kudela *et al.*, 2000; Badruddin, 2006; Kudela, 2008), 'long-lived geomagnetic storms', caused by multiple subregions of southward magnetic field within a complex solar-wind flow (Xie *et al.*, 2006) and 'multiple-dip geomagnetic storms' (Kudela and Storini, 2005; Zhang, Richardson, and Webb, 2008) are of considerable space weather consequence.

These effects of different magnitude, time profile and duration are expected to be produced due to stream structures of different plasma and field configuration, duration and speed profiles. The present catalog and analysis are expected to be useful in such studies and other related ones.

2. Data and Analysis

Instruments onboard spacecraft have been detecting high-speed streams in the solar wind since the early sixties. Then with the launch of a new class of space missions (*Helios*, *Voyager*, *Pioneer*, *Ulysses*), equipped with new generation of instruments, from mid-1970s,

provided impetus to solar, heliospheric and solar-terrestrial research. Another step forward occurred in mid-1990s with the launch of *Yohkoh*, SOHO, WIND, ACE and TRACE spacecraft (Schwenn, 2006). With all these spacecraft in space, the pioneering efforts of King and Papitashvili (http://omniweb.gsfc.nasa.gov) in putting the multi-source solar-wind plasma and field data and related parameters in conveniently usable format have given further boost to research in heliospheric science and related areas, and innumerable studies have utilized this long series of data sets from the mid-1960s. One of the pieces of information of great use to the solar-terrestrial physics community has been the identification of high-speed solar-wind streams from this OMNI data set (*e.g.*, Lindblad and Lundstedt, 1981, 1983; Lindblad, Lundstedt, and Larsson, 1989; Mavromichalaki, Vassilaki, and Marmatsouri, 1988; Mavromichalaki and Vassilaki, 1998) for solar cycles 20 – 22 (1964 – 1996). Identified streams have been utilized and analyzed earlier (*e.g.*, Badruddin, 1997; Shrivastava and Jaiswal, 2003; Maris and Maris, 2005; and many others).

With the availability of better quality and more continuous records, with lesser data gaps, of solar, interplanetary and near-Earth data lead us to identify the streams in the solar wind, their sources, and properties and associated features. On critical examination, use and analysis of the solar, heliospheric and near-Earth observations, we have observed that a high-speed stream in the solar wind (from the start of a stream till its complete/near-complete recovery) may be a consequence of *i*) a high-speed CME, *ii*) high-speed plasma from a coronal hole, *iii*) multiple CMEs occurring in succession before a near-complete recovery to normal level, *iv*) multiple coronal holes, and *v*) a compound stream due to both the CMEs and the CH. In this way we have adopted this new notion and classified all the streams, based on the source, into five classes.

3. Selection of High-Speed Streams

In this study we consider a solar-wind stream as a high-speed stream when there is considerable enhancement ($\Delta V \geq 100$ km s^{-1}) in plasma speed from the pre-increase level, which persists for at least two days after the onset. The start time of the stream is taken as the time (hour) when the solar plasma speed starts increasing towards maximum (V_{m}) and the end time is taken as the time when the speed decreases to almost pre-enhancement level.

We have listed streams of solar cycle 23 (1996 – 2007) satisfying the above criteria in Table 1 (electronic supplementary material). These streams have been identified using the hourly solar-wind plasma and field values and plots generated from the OMNI dataset (http://omniweb.gsfc.nasa.gov). In this Table 1 we have listed the start time (the time when a stream starts rising) and the end time as the time when the stream's speed comes down, for the first time, to pre-increase level or to a lowest constant speed level after the initial rise and fall in its velocity. We have also listed in this table the stream duration, which is the time difference between the start and end time of the stream. Then we have listed the identified source(s) of stream (coronal hole(s)/CME(s)) which may be due to *i*) a single coronal hole, *ii*) a single CME, *iii*) multiple coronal holes, *iv*) multiple CMEs, and also *v*) it may be a 'compound' stream due to coronal hole(s) and CME(s). As representative examples of these five types of streams, based on their source(s), we have plotted them in Figures 1 – 5, showing variations in their plasma and field parameters.

To distinguish between sources (CH or CME) of streams, we have identified them from the differences in the time profiles of plasma speed, temperature, and density and associated magnetic field (see Burlaga, 1975; Iucci *et al.*, 1979; Mavromichalaki and Vassilaki, 1998; Gosling, 1996). In order to distinguish between CH- and CME-related high-speed streams

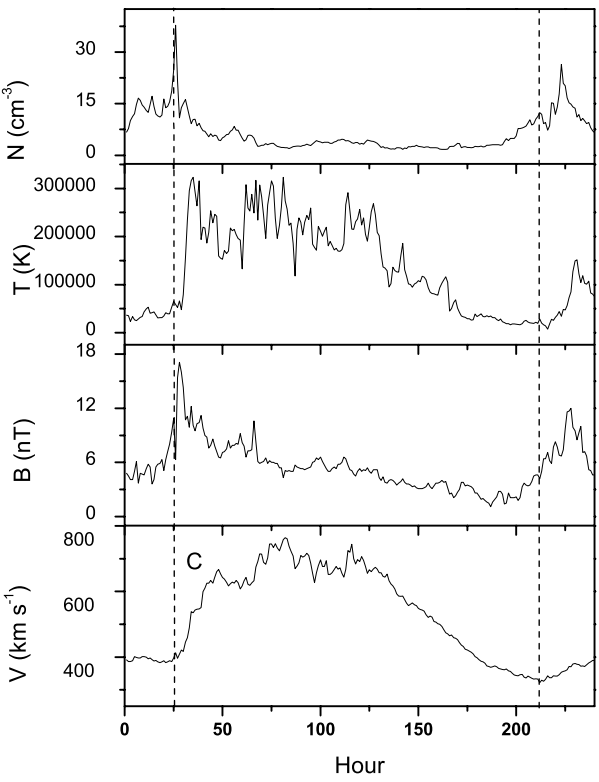

Figure 1 A typical high-speed stream (HSS) due to a single coronal hole (UT 20:00, 5 March 2005 to UT 20:00, 13 March 2005). The dashed lines on the left and right indicate the start and the end of the stream.

(HSS), we looked at the following broad distinctions: *i*) during CH-HSS, enhancement in solar-wind speed proceeds relatively slowly to reach its peak and remains enhanced for a longer period before it comes down slowly, while during CME-HSS, velocity increases at a faster rate to reach its peak and remains enhanced for a shorter period and comes down relatively faster, *ii*) proton density rises to unusually high values near (often preceding) the leading edges of streams due to CH, while its enhancement is almost simultaneous to velocity enhancement due to CME streams, *iii*) during CH-HSS, proton temperature varies in a pattern similar to the flow speed, while temperature becomes low during CME after the initial rise during shock, if present (shock is likely to form during the passage of fast ICMEs), *iv*) magnetic field and proton density peak before the speed maximum during CH-HSS, while peaks in these three interplanetary parameters are near simultaneous during CME-HSS. Published data on ICMEs/CIRs (*e.g.*, Cane and Richardson, 2003; Manoharan *et al.*, 2004; Jian *et al.*, 2006a, 2006b) and SOHO/ACE/WIND websites were of further help in identifying the stream sources.

We have listed in this table the number of events (coronal hole/CME) the complete stream is due to. Since the Earth's magnetosphere responds to dynamic changes in the solar/solar-wind input and shocks play an important role in solar-terrestrial physics research, *e.g.*, in mediating and influencing the energy and momentum balance (Tsurutani *et al.*, 1988, 1999; Badruddin, 2002; Schwartz, 2006), we have also listed ('Y') if shock(s) is (are) identified either by ACE/WIND (A/W) and/or sudden storm commencement (SSC) during a particular stream. In the column 'stream structure', we have indicated the sources (C/E), their numbers as well as shocks(s), if present, during the whole stream. It is believed that SSC is a geo-

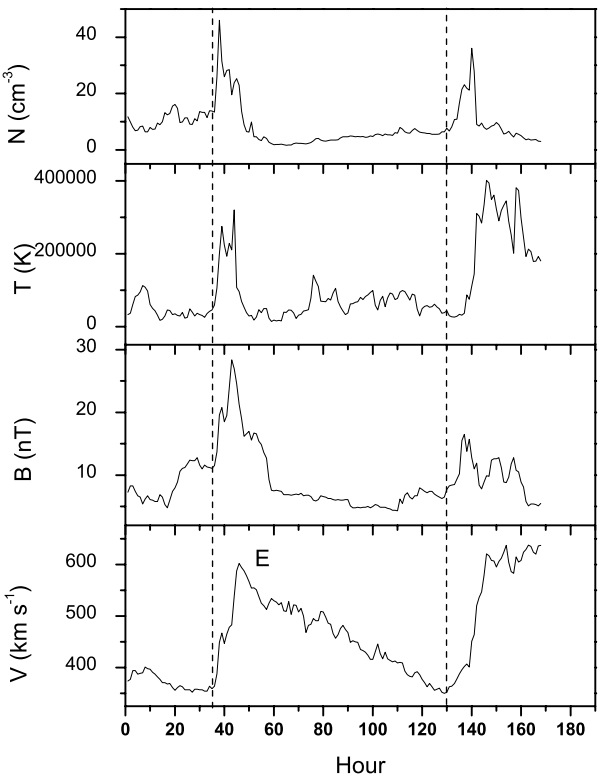

Figure 2 A typical HSS due to a single mass ejection stream (UT 08:00, 22 September 1999 to UT 06:00, 26 September 1999). The dashed lines on the left and right indicate the start and the end of the stream.

magnetic signature of the passage of shock; it signals the arrival of an interplanetary shock structure at the Earth (Smith, 1983; Gonzalez *et al.*, 1994).

A subset of CMEs called magnetic clouds (Burlaga *et al.*, 1981; Klein and Burlaga, 1982) is of special importance in the area of solar-terrestrial physics (*e.g.*, Zhang and Burlaga, 1988; Lepping *et al.*, 1991; Badruddin, 1998; Zhang *et al.*, 2004; Singh and Badruddin, 2007b; Gopalswamy *et al.*, 2008). We have indicated in the table if a CME has magnetic cloud structure by the symbol 'Y' under 'Magnetic cloud' column. Then, some of the plasma and field parameters are also listed in the table, which provide information about some specific features of the streams. In the last four columns, the peak values of solar plasma/field parameters, velocity (V_{max}), density (N_{max}), temperature (T_{max}) and magnetic field (B_{max}) during each stream are also given.

4. Statistical Distribution and Plasma/Field Parameters of High-Speed Streams During Solar Cycle 23

It is important to know the distribution and plasma/field properties of streams for the studies related to solar-terrestrial/space weather effects. Since the sources, duration and speed of streams are important to decide their effectiveness in producing the geomagnetic (see, *e.g.*, Xie *et al.*, 2006; Zhang, Poomvises, and Richardson, 2008; Badruddin and Singh, 2009; Gupta and Badruddin, 2009), ionospheric disturbances (Marcz, 1992; Burns *et al.*, 2007) and Forbush decrease in cosmic rays in the heliosphere (Lockwood, 1971; Venkatesan and

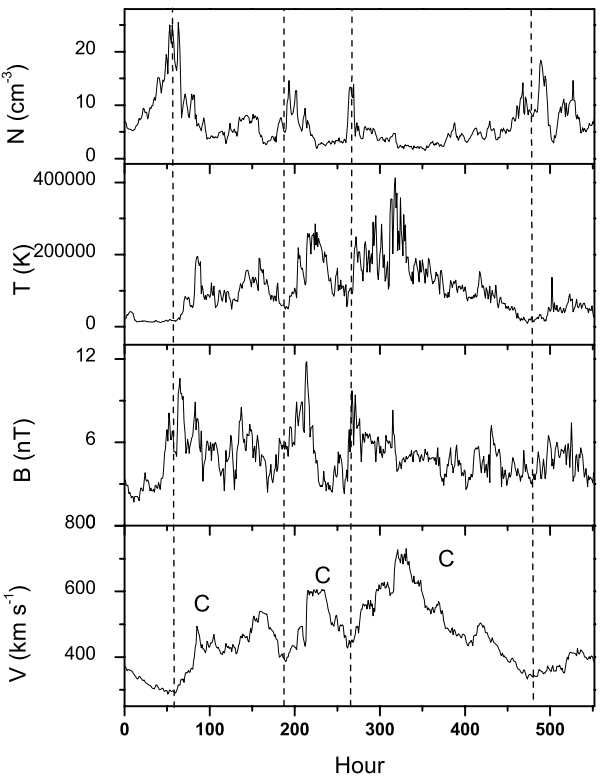

Figure 3 A typical HSS caused by multiple streams from coronal holes (UT 00:00, 8 April 1996 to UT 00:00, 26 April 1996). The dashed lines at extreme left and right indicate the start and end of the stream. Dashed lines in between indicate the additional source(s) during stream.

Badruddin, 1990; Badruddin, 1997; Cane, 2000; Singh and Badruddin, 2007b), we have studied separately the distribution and plasma/field properties of streams classified on the basis of their origin, speed as well as duration. It is expected that the knowledge of statistical behaviors of the streams in such a manner will stimulate further studies in the related area of space physics in general and solar-terrestrial physics, in particular.

4.1. Streams of Different Solar Source(s)

Cane and Richardson (2003) identified ICMEs in the near-Earth solar wind during 1996 – 2002 and tabulated them along with certain plasma and field properties. Jian *et al.*, (2006a, 2006b) have listed plasma and field properties associated not only with ICMEs but also with SIRs observed at 1 AU during 1995 – 2004. These catalogs are useful for the study of their behavior and properties during different solar activity periods and to study the effects of individual ICMEs and stream interaction regions (SIRs) in the interplanetary space. In addition to covering an extended period (1996 – 2007) of almost a complete solar cycle (Cycle 23), our approach to prepare a catalog of high-speed streams, Table 1, although complementary to Cane and Richardson (2003) and Jian *et al.*, (2006a, 2006b) in some sense, is significantly different from them.

Solar-wind velocity (V) plays a crucial role in many solar/interplanetary effects, *e.g.* the dawn-to-dusk electric field ($-\mathbf{V} \times \mathbf{B}_z$) in solar wind-magnetosphere coupling phenomena (see Burton, McPherron, and Russel, 1975; Tsurutani and Gonzalez, 1997), and convection by solar wind in modulating cosmic rays (see Venkatesan and Badruddin, 1990). In addi-

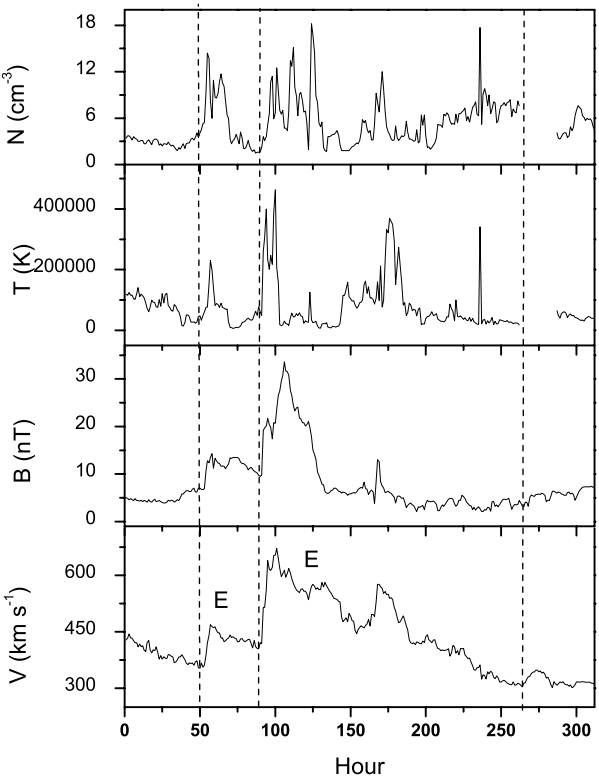

Figure 4 A typical HSS caused by multiple mass ejections (UT 00:00, 10 August 2000 to UT 00:00, 19 August 2000). The dashed lines at extreme left and right indicate the start and end of the stream. Dashed lines in between indicate the additional source(s) during stream.

tion, the 'geo-effectiveness' and 'cosmic-ray effectiveness' in the amplitudes and time profiles of geomagnetic and cosmic-ray storms are expected to be different for different stream structures, *e.g.*, streams due to single ICMEs/SIRs, streams and structures evolved due to two or more interacting ICMEs and/or SIRs (*e.g.*, see Burlaga, Behannon, and Klein, 1987; Badruddin and Singh, 2009; Gupta and Badruddin, 2009). Further, field topology and complexity varies from stream to stream depending upon the structure itself as well as on interacting structures; it also affects, *e.g.*, the 'geo-effectiveness' and 'cosmic-ray effectiveness'. In this way we have catalogued the high-speed streams and identified the structures influencing the time profile and amplitudes of stream; an approach different from those of Cane and Richardson (2003) and Jian *et al.*, (2006a, 2006b).

Regarding the stream catalog (Table 1), it must be clarified that we have not tabulated those streams where there is a data gap in the plasma and field parameters, required for identification of streams, to the extent that it becomes difficult to put them in one category or the other. However, they are not so many in number that they influence our statistical conclusions.

Classification of solar-wind drivers of geospace consequences into different categories, based on their solar sources and evolutions in the interplanetary space, has been done in recent past (*e.g.*, Richardson, Cliver, and Cane, 2000; Bothmer and Zhukov, 2006; Zhang *et al.*, 2007; Echer *et al.*, 2008). Depending upon source(s), we have divided the high-speed solar-wind stream into five groups, namely those associated with *i*) a single coronal hole (SCH), *ii*) a single mass ejection (SME), *iii*) multiple coronal holes (MCH), *iv*) multiple

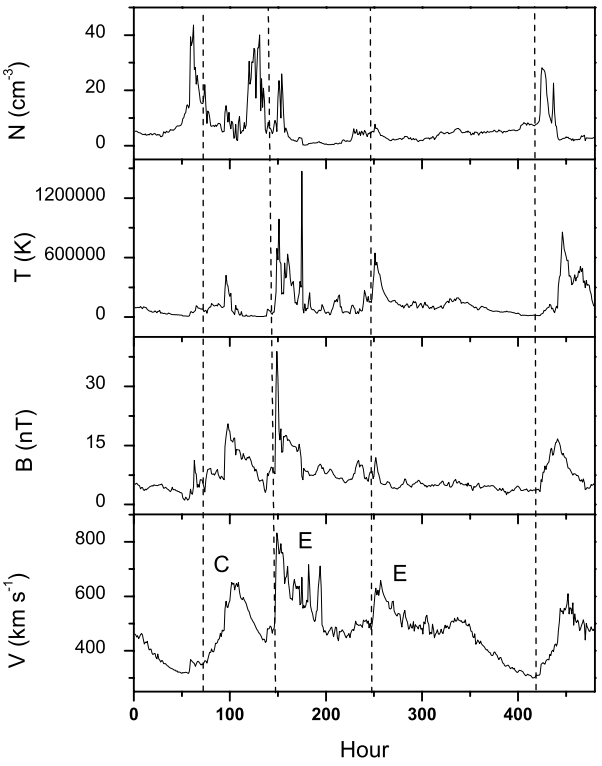

Figure 5 A typical HSS as a result of a compound stream associated with a coronal hole and a CME (UT 00:00, 30 April 1998 to UT 12:00, 15 May 1998). The dashed lines at extreme left and right indicate the start and end of the stream. Dashed lines in between indicate the additional source(s) during the stream.

Table 2 Yearly distribution of HSS of different solar source(s) during 1996 – 2007.

Solar source (s)	1996	1997	1998	1999	2000	2001	2002	2003	2004	2005	2006	2007
Single CH	25	6	17	17	16	11	20	12	19	23	24	10
Multiple CH	12	4	6	8	4	3	7	12	12	3	4	9
Single ME	–	4	3	8	5	3	3	–	3	4	7	2
Multiple ME	–	1	1	1	6	6	1	1	2	2	0	0
Compound	3	12	13	12	12	15	12	11	7	8	5	8
Total	40	27	40	46	43	38	43	36	43	40	40	29

mass ejections (MME), and *v*) compound streams associated with both coronal hole(s) and mass ejection(s) (CMP), respectively.

The distribution of these different groups of streams in different years of cycle 23 is given in Table 2. Out of the total 465 streams identified in solar cycle 23 (1996 – 2007), in order of decreasing number, 43% of the streams belong to single coronal hole (SCH) group, 26% to compound (CMP) group, 18% to multiple coronal holes (MCH), 9% to a single mass ejection (SME) and 4% of them are from multiple mass ejections (MME) group of streams (see Figure 6).

In earlier studies of high-speed streams, Lindblad and Lundstedt, (1981, 1983) and Lindblad, Lundstedt, and Larsson (1989) in three papers compiled high-speed streams observed

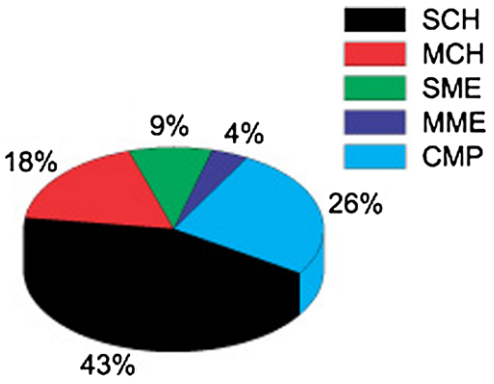

Figure 6 Pie chart illustrating the number (%) of HSS of solar cycle 23 (1996 – 2007) with solar source(s), *i.e.* single coronal hole (SCH), multiple coronal holes (MCH), single coronal mass ejection (SME), multiple mass ejections (MME) and compound stream due to both coronal hole(s) and coronal mass ejection(s) (CMP).

Table 3 Number of high-speed streams as classified according to their solar origin, during minimum, increasing, maximum and decreasing years in the period 1996 – 2007.

SCH – single C; MCH – multiple C; SME – single E; MME – multiple E; CMP – mix C & E.

Phases	SCH	MCH	SME	MME	CMP
Minimum	59	25	9	0	16
Increasing	40	18	15	3	37
Maximum	47	14	11	13	39
Decreasing	54	27	8	4	26
Total	200	84	43	20	118

by near-Earth spacecraft in the periods 1964 – 1975, 1975 – 1978, and 1978 – 1982 (solar cycles 20, and partly 21). These streams were classified into corotating and so-called flare-generated streams. Mavromichalaki and Vassilaki (1998) also presented a catalog of high-speed streams for the period 1985 – 1996 (cycle 22) as a continuation of a similar previously published catalog (Mavromichalaki, Vassilaki, and Marmatsouri, 1988) for the period 1972 – 1984; they also classified them into corotating and flare-generated streams. By plotting the number of corotating and flare-generated streams for each year from 1964 to 1996 (solar cycles 20 – 22), it was previously observed (Mavromickalaki and Vassilaki, 1998) that the number of flare-generated streams are more around the solar maximum while corotating streams are more around the solar minimum. However, another statistical study (Maris and Maris, 2005) of corotating and flare-generated streams of the period 1964 – 1996 (solar cycles 20 – 22) concluded that the frequency of streams was higher during the declining and minimum phases of cycles 20, 21, and 22, regardless of their solar sources (coronal holes/solar flares).

It is also of interest to know the distribution of streams, classified by us, during different activity levels of the solar cycle. For this purpose we have divided solar cycle 23 in to four phases, namely, low or minimum (1996, 2006 and 2007), increasing or rising (1997, 1998 and 1999), high or maximum (2000, 2001 and 2002) and declining or decreasing (2003, 2004 and 2005) phases of solar cycle.

Out of the total 200 single coronal holes (SCH) group of streams (see Table 3), the majority of them (57%) were observed during decreasing and minimum phases of solar activity cycle (Figure 7a). A similar trend in the distribution of multiple coronal holes (MCH) group of streams is apparent as 62% of them were observed during decreasing and minimum phase of solar cycle (Figure 7b). The trend in distribution of streams for the other three groups of streams is different, *i.e.* single mass ejection (SME), multiple mass ejections (MME) and

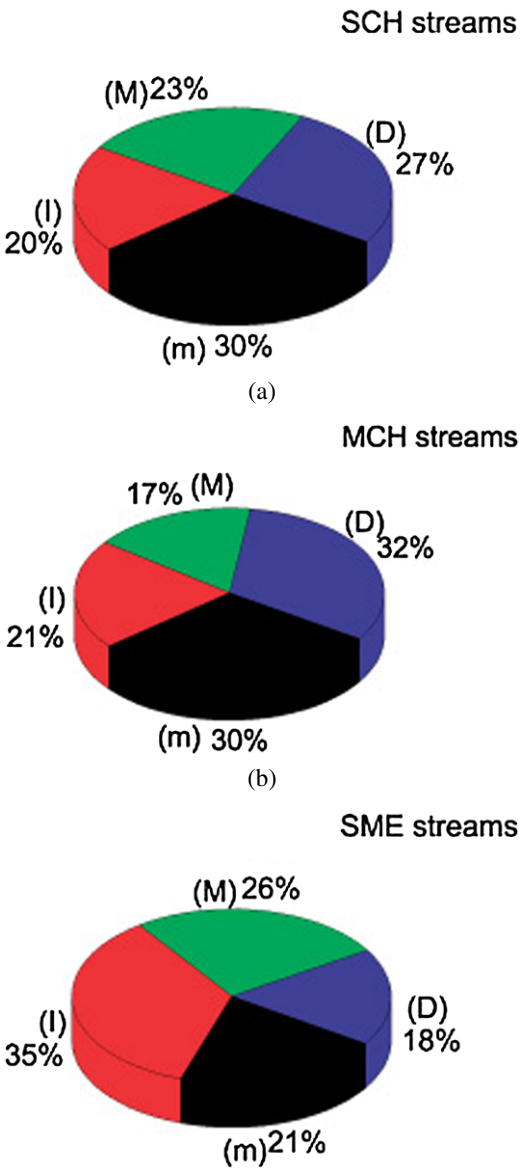

Figure 7 Pie chart showing the occurrence of HSS due to various types of streams classified on the basis of their source(s), during minimum (m), increasing (I), maximum (M), and decreasing (D) phases of solar activity during 1996 – 2007.

compound (CMP) streams; the majority of streams in these categories were observed during increasing and maximum phases of solar cycle. Specifically, 61% of all SME streams, 80% of all MME streams and 64% of all CMP streams were observed during increasing and maximum phase of solar cycle (see Figures 7c – 7e). It is worth mentioning here that the CMEs are more frequent during a sunspot maximum (Gopalswamy, 2006), while corotating interaction regions (CIRs) occur when solar activity is declining (Kane, 2007).

Since plasma density and temperature profiles provide information about the physical conditions within the streams, and plasma speed and associated field strength both are im-

Figure 7 (*Continued.*)

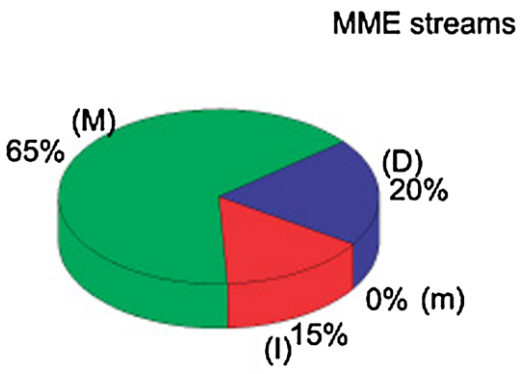

(d)

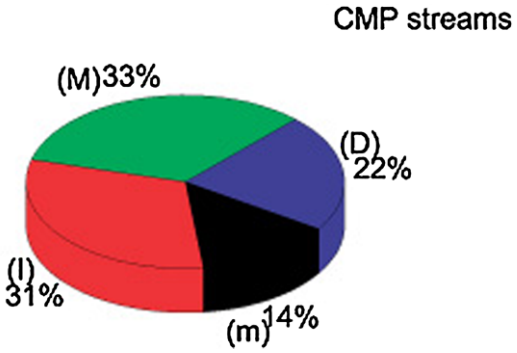

(e)

Table 4a Yearly averaged peak values of solar plasma/field parameters during HSS associated with single coronal hole during 1996 – 2007.

Plasma/field parameters	1996	1997	1998	1999	2000	2001	2002	2003	2004	2005	2006	2007
$\langle V_{max} \rangle$ (km s^{-1})	553	480	539	541	546	531	542	600	561	620	578	623
$\langle N_{max} \rangle$ (cm^{-3})	25.0	21.7	21.9	27.1	25.7	29.3	26.5	19.2	15.7	32.3	24.8	29.0
$\langle T_{max} \rangle$ (10^5 K)	2.5	1.9	3.2	3.0	3.0	2.9	3.0	3.9	2.5	3.8	2.9	3.3
$\langle B_{max} \rangle$ (nT)	11.2	10.5	13.9	14.0	14.4	14.8	15.6	14.3	12.4	20.5	13.3	12.4

portant parameters, in addition to sources, in determining the 'geo-effectiveness' as well short-term modulation of cosmic rays ('cosmic-ray effectiveness'), we have determined the averages of peak values of these plasma and field parameters in different years of cycle 23 (see Tables 4a – 4e). These tables provide an overview of variations in averaged maxima of various parameters during different years of varying level of solar activity. These tabulated values also provide information about the variations in respective parameters in different years due to streams of different types.

Jian *et al.*, (2006a, 2006b) have calculated certain interplanetary parameters (maximum field strength, change in speed *etc.*) from 1995 to 2004 for each year during the passage of stream interaction regions (SIRs) and ICMEs. Our results (Tables 4a to 4e), in addition,

Table 4b Yearly averaged peak values of solar-wind parameters for the multiple CH-type streams during 1996 – 2007.

Plasma/field parameters	1996	1997	1998	1999	2000	2001	2002	2003	2004	2005	2006	2007
$\langle V_{max} \rangle$ (km s^{-1})	573	720	588	598	662	527	638	741	637	613	617	639
$\langle N_{max} \rangle$ (cm^{-3})	30.2	37.0	29.5	21.5	33.0	37.0	32.8	25.0	19.2	29.7	30.5	31.4
$\langle T_{max} \rangle$ (10^5K)	3.3	2.6	2.9	3.9	4.9	3.7	4.4	4.8	4.5	3.7	3.6	3.4
$\langle B_{max} \rangle$ (nT)	12.1	13.5	13.8	15.2	16.5	20.6	16.8	16.2	13.2	17.0	14.2	14.5

Table 4c Yearly averaged peak values of solar-wind parameters for the single ME-type streams during 1996 – 2007.

Plasma/field parameters	1996	1997	1998	1999	2000	2001	2002	2003	2004	2005	2006	2007
$\langle V_{max} \rangle$ (km s^{-1})	–	490	453	585	512	577	483	–	556	790	597	480
$\langle N_{max} \rangle$ (cm^{-3})	–	30.7	24.7	19.5	29.0	16.0	23.3	–	21.0	24.7	42.0	25.0
$\langle T_{max} \rangle$ (10^5K)	–	3.9	1.5	3.8	2.0	1.6	2.9	–	2.3	5.7	3.8	1.7
$\langle B_{max} \rangle$ (nT)	–	20.0	14.7	17.1	23.0	17.7	18.3	–	13.3	24.0	15.7	10.3

Table 4d Yearly averaged peak values of solar-wind parameters for the multiple ME-type streams during 1996 – 2007.

Plasma/field parameters	1996	1997	1998	1999	2000	2001	2002	2003	2004	2005	2006	2007
$\langle V_{max} \rangle$ (km s^{-1})	–	590	850	870	668	765	680	760	845	875	–	–
$\langle N_{max} \rangle$ (cm^{-3})	–	33.0	15.0	44.0	23.7	41.5	33.0	14.0	17.0	36.5	–	–
$\langle T_{max} \rangle$ (10^5K)	–	4.2	9.0	5.1	3.9	3.9	5.7	1.0	3.8	3.5	–	–
$\langle B_{max} \rangle$ (nT)	–	27	29	24	20.5	42	30	20	26	21	–	–

Table 4e Yearly averaged peak values of solar-wind parameters for the compound streams during 1996 – 2007.

Plasma/field parameters	1996	1997	1998	1999	2000	2001	2002	2003	2004	2005	2006	2007
$\langle V_{max} \rangle$ (km s^{-1})	513	533	597	622	660	597	630	770	600	697	676	674
$\langle N_{max} \rangle$ (cm^{-3})	24.7	36.8	35.2	31.3	31.2	32.7	32.0	22.4	32.0	39.0	25.0	36.0
$\langle T_{max} \rangle$ (10^5K)	2.1	2.8	4.4	4.3	4.0	4.2	3.3	5.9	4.4	3.7	4.9	4.2
$\langle B_{max} \rangle$ (nT)	12.7	15.5	21.4	17.4	25.3	18.9	19.5	22.3	23.4	23.8	16.2	16.6

provide the averaged peak values of a number of plasma/field parameters during five types of streams for each year from 1996 to 2007.

The solar-wind maximum speed obtained from near-Earth data for each year from 1965 – 1987 (Storini and Fillici, 1994) shows peaks in declining phase of solar cycle 20 (1973 – 1974) and near/after maximum of cycle 21 (1982). However, the averaged magnetic field is high in 1972 and 1982; the years near/after solar maximum years of cycle 20 and 21.

Table 5 Comparison of averaged values of solar-wind parameters due to streams of different origin observed in 1996 – 2007.

Solar source	$\langle V_{\max} \rangle$ (km s^{-1})	$\langle N_{\max} \rangle$ (cm^{-3})	$\langle T_{\max} \rangle$ (10^5K)	$\langle B_{\max} \rangle$ (nT)
SCH	559 ± 6.84	24.8 ± 0.92	3.0 ± 0.10	13.9 ± 0.30
MCH	629 ± 10.92	29.7 ± 1.44	3.8 ± 0.17	15.3 ± 0.46
SME	552 ± 19.13	25.6 ± 2.14	2.9 ± 0.33	17.4 ± 1.29
MME	767 ± 38.26	28.6 ± 3.03	4.4 ± 0.50	26.6 ± 2.90
CMP	631 ± 11.43	31.5 ± 1.27	4.0 ± 0.19	19.4 ± 0.82

Maris and Maris (2005) analyzed maximum velocities of high-speed streams during different phases (minimum, ascending, maximum and descending) of solar cycles 20 – 22. Their results show that maximum speed is generally higher during a maximum phase of each cycle for the so-called flare-generated streams, while they are in general, higher in number during descending phases of cycle 20, 21 and 22 for CIR-generated streams.

A comparison of maximum values of respective parameters (V, N, T, and B) due to different types of streams for the whole cycle is also of interest. These values are given in Table 5. We see from this table that the averaged parameters $\langle V_{\max} \rangle$, $\langle N_{\max} \rangle$, $\langle T_{\max} \rangle$, and $\langle B_{\max} \rangle$ are comparatively higher during multiple interacting groups, particularly multiple mass ejections (MME) and the compound (CMP) group of streams. Thus, such types of stream are likely to be more 'geo-effective' and 'cosmic-ray effective' as found in certain studies (*e.g.*, Burlaga, Behannon, and Klein, 1987; Cliver, Drodge, and Muller-Mellin, 1993; Echer and Gonzalez, 2004).

4.2. Streams of Different Speed

The speed of solar-wind stream is an important parameter, apart from its source and structure in the interplanetary space, and plays an important role in solar-terrestrial/space weather effects (Gosling *et al.*, 1990; Badruddin, 1998; Srivastava and Venkatakrishnan, 2002; Ballatore, 2002). We have divided the streams according to their maximum speed near 1 AU into three groups: *i*) 400 km s^{-1} $< V_{\max} \leq$ 550 km s^{-1}, *ii*) 550 km s^{-1} $< V_{\max} \leq$ 650 km s^{-1}, and *iii*) $V_{\max} >$ 650 km s^{-1}, and we designated them as lower-range high-speed stream (LR-HSS), medium-range high-speed stream (MR-HSS) and higher-speed high-speed stream (HS-HSS). After this division into three suitable groups, we observe that out of a total 465 HSS, 36% of the streams (see Figure 8) are in the lower range of speed (400 km s^{-1} $< V_{\max} \leq$ 550 km s^{-1}), 34% in the medium range of speed (550 km s^{-1} $< V_{\max} \leq$ 650 km s^{-1}) and rest 30% have higher range of speed ($V_{\max} >$ 650 km s^{-1}). These arbitrary criteria divide all the HSS into three groups encompassing almost an equal number (about one third) in each speed group.

It is also of interest to know the distribution of streams of different speed group during different years of solar cycle. The number of streams into three groups, divided according to their maximum speed, is given in Table 6. It is also useful to know the number of streams of different speed range in different phases of solar cycle. As plotted in Figures 9a – 9c, the frequency of lower-range HSS (LS) is higher during increasing (35%) and maximum (31%) phases, medium-range streams (MS) are almost equally distributed during different phases, while higher-speed HSS (HS) are more frequent (38%) in the declining phase of solar cycle 23 (also see Table 7) as compared to other phases.

In order to provide a broader perspective of distribution of HSS, the frequency histogram of all the streams observed in solar cycle 23 has also been plotted by dividing them into bins

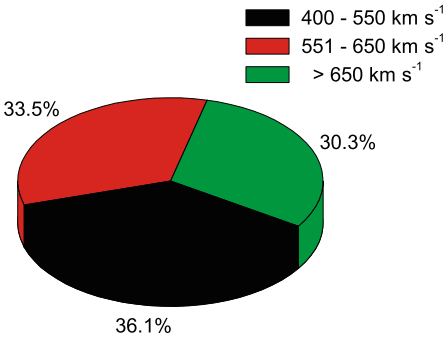

Figure 8 Pie chart showing the number (in percent) of HSS of lower speed (LS), medium speed (MS) and higher speed (HS) in solar cycle 23.

Table 6 Yearly distribution of high-speed streams of different speed interval during 1996 – 2007.

Speed ($km\,s^{-1}$)	1996	1997	1998	1999	2000	2001	2002	2003	2004	2005	2006	2007
400 – 550	18	17	23	19	16	13	23	03	13	06	12	05
551 – 650	16	09	10	15	15	14	08	11	20	12	17	09
> 650	06	01	07	12	12	11	12	22	10	22	11	15
Total streams	40	27	40	46	43	38	43	36	43	40	40	29

Table 7 Number of HSS, as classified according to their speed, during various phases in solar activity during 1996 – 2007.

Phases	LS	MS	HS
Minimum	35	42	32
Increasing	59	34	20
Maximum	52	37	35
Decreasing	22	43	54
Total	168	156	141

LS – lower speed; MS – medium speed; HS – higher speed.

of 50 $km\,s^{-1}$ (see Figure 10). The number of streams increases from the 400 – 450 $km\,s^{-1}$ bin to 551 – 600 $km\,s^{-1}$ bin, and then it decreases slowly up to the 651 – 700 $km\,s^{-1}$ bin and then a decline in number of faster events is evident, as streams beyond 700 $km\,s^{-1}$ are fewer in number.

It will be useful to know about the distribution of average of the peak values of different plasma/field parameters, especially V, N, T and B, during the streams of different speed ranges. These parameters are given in Tables 8a – 8c. A comparison of these parameters due to streams of three speed ranges provides us with an interesting observation; the average values of temperature and field strength are lower for low-range HSS, increases for medium-range HSS and their values are highest for high-range HSS, increasing in accordance with speed range. However, such a systematic increase is not observed in density maxima (see Table 9).

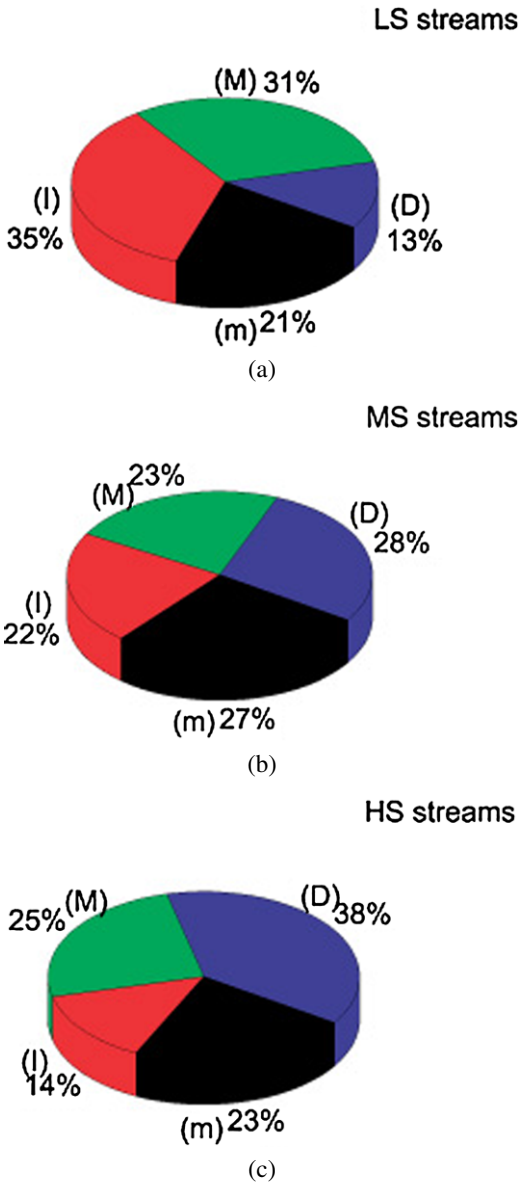

Figure 9 Pie chart showing the occurrence of HSS, classified according to their speed (LS, MS and HS streams) during various phases of solar activity, *i.e.* minimum (m), increasing (I), maximum (M) and decreasing (D) phases.

4.3. Streams of Different Duration

There are some studies which demonstrate the possibility that the duration of the streams, especially those from coronal holes (see, *e.g.*, Filisetti *et al.*, 1988; Iucci *et al.*, 1979), might be related to the amplitude and the duration for which the effects of streams persist. Thus, we thought it prudent to study the statistical distribution of streams of different durations. For this purpose we divided the streams of solar cycle 23 into *i*) short-duration HSS ($\Delta T \leq 4$ days), *ii*) medium-duration HSS (4 days $< \Delta T \leq 8$ days), and *iii*) long-duration HSS ($\Delta T > 8$ days). The distributions of streams of different durations in different years

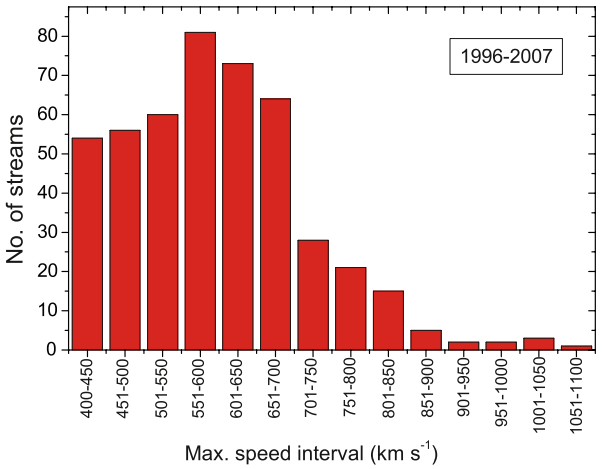

Figure 10 Speed distribution of HSS observed during 1996 – 2007.

Table 8a Values of averaged solar plasma/field parameters in different years during lower speed streams in the period 1996 – 2007.

Plasma/field parameters	1996	1997	1998	1999	2000	2001	2002	2003	2004	2005	2006	2007
$\langle V_{max} \rangle$ (km s^{-1})	481	478	486	481	465	484	486	493	499	460	486	498
$\langle N_{max} \rangle$ (cm^{-3})	26.7	30.2	27.1	24.0	25.1	26.3	27.6	17.3	18.9	18.8	24.9	23.6
$\langle T_{max} \rangle$ (10^5K)	2.0	2.4	2.5	2.2	1.9	2.7	2.5	2.3	2.1	2.0	2.1	1.9
$\langle B_{max} \rangle$ (nT)	10.7	14.2	14.8	13	15.9	15.2	14.8	13.7	11.4	12.2	12.6	9.5

Table 8b Averaged solar parameters in different years during medium speed streams in the period 1996 – 2007.

Plasma/field parameters	1996	1997	1998	1999	2000	2001	2002	2003	2004	2005	2006	2007
$\langle V_{max} \rangle$ (km s^{-1})	591	586	613	617	602	597	604	616	591	603	607	616
$\langle N_{max} \rangle$ (cm^{-3})	26.8	37.6	23.5	26.5	23.9	38.8	31.2	22.1	22.6	35.8	29.6	34.4
$\langle T_{max} \rangle$ (10^5K)	3.2	3.4	4.2	4.3	3.5	4.2	4.2	4.3	3.1	3.5	3.4	3.3
$\langle B_{max} \rangle$ (nT)	12.0	16.8	17.2	16.1	17.8	19.1	18.4	15.3	16.2	17.0	14.2	14.5

Table 8c Averaged solar parameters in different years during higher-speed streams in the period 1996 – 2007.

Plasma/field parameters	1996	1997	1998	1999	2000	2001	2002	2003	2004	2005	2006	2007
$\langle V_{max} \rangle$ (km s^{-1})	688	710	764	717	784	764	749	775	755	754	702	687
$\langle N_{max} \rangle$ (cm^{-3})	25.3	25.0	34.0	29.7	37.1	31.4	30.4	22.5	15.1	35.2	28.8	32.2
$\langle T_{max} \rangle$ (10^5K)	3.7	3.9	6.1	5.3	5.5	4.2	4.4	5.4	5.7	3.8	4.7	4.1
$\langle B_{max} \rangle$ (nT)	12.9	16.0	22.6	20.2	26.2	31.5	21.8	19.2	17.9	20.5	15.5	15.3

Table 9 Comparison of averaged values of solar plasma/ field parameters due to streams of three speed ranges; lower speed (LS), medium speed (MS) and higher speed (HS) observed during 1996 – 2007.

Speed	$\langle V_{max} \rangle$ (km s^{-1})	$\langle N_{max} \rangle$ (cm^{-3})	$\langle T_{max} \rangle$ (10^5K)	$\langle B_{max} \rangle$ (nT)
LS	483 ± 3.25	24.2 ± 0.88	2.2 ± 0.07	13.2 ± 0.31
MS	604 ± 2.33	29.4 ± 1.14	3.7 ± 0.11	16.2 ± 0.48
HS	737 ± 7.38	28.9 ± 1.30	4.7 ± 0.17	19.9 ± 0.89

Table 10 Year-wise distribution of HSS of different duration observed in 1996 – 2007.

Stream duration (days)	1996	1997	1998	1999	2000	2001	2002	2003	2004	2005	2006	2007
< 4	02	01	08	12	07	04	04	02	09	02	03	–
4 – 8	29	11	19	24	21	11	22	13	14	15	22	11
> 8	09	15	13	10	15	23	17	21	20	23	15	18
Total	40	27	40	46	43	38	43	36	43	40	40	29

of solar cycle are given in Table 10. Out of the total 465 streams, short-duration ($\Delta T \leq 4$ days) HSS are 12%, medium-duration streams (4 days $< \Delta T \leq 8$ days) are 46%, and long-duration streams ($\Delta T > 8$ days) are 43% (Figure 11). As this distribution in different groups, according to duration, is arbitrary, we studied the frequency distribution of streams of different durations by dividing the streams into different bins of 2 hours duration and plotted their distribution. As shown in Figure 12, the number of streams rises initially up to a maximum number in a 6 – 7 hour bin and then the number falls almost exponentially as the duration of the streams increases.

Mavromichalaki and Vassilaki (1998) studied the distribution of the stream duration and observed that most of the streams are of 4 – 6 day duration during cycle 20 – 22. Our results for cycle 23, with less data gaps, show (Figure 12) that the number of streams of duration 7 – 9 days is also quite large in addition to streams of 4 – 6 day duration.

We also compare the relative distribution of short-duration, medium-duration and long-duration HSS during the increasing, maximum, decreasing and minimum phases of solar activity. We observe that (see Figure 13) comparatively the short-duration streams are higher in number during the increasing phase (Figure 13a), medium-duration streams are smaller in number during the declining phase (Figure 13b), while the long-duration stream are relatively more frequent during the maximum and decreasing phases of solar cycle 23 (also see Table 11).

We have also calculated the averages of peak values of different plasma/field parameters (V, N, T, and B) due to streams of different groups classified on the basis of their duration, *i.e.*, short-, medium- and long-duration streams. These values in different years for different duration-range streams are given in Tables 12a – 12c. A comparison of these parameters during streams of different duration-range shows that, on an average basis, the maximum values of V, N, T and B increase with increasing duration (Table 13), *i.e.*, these parameters ($\langle V_{max} \rangle$, $\langle N_{max} \rangle$, $\langle T_{max} \rangle$, $\langle B_{max} \rangle$) are lowest for short-duration streams, have intermediate values for medium-duration stream, and are highest for long-duration stream. Since longer-duration streams mostly involve interactions between two or more streams, these interplanetary parameters are probably enhanced as a result of interactions between them. Moreover, the chances of interactions between streams will be higher when at least one of them is faster.

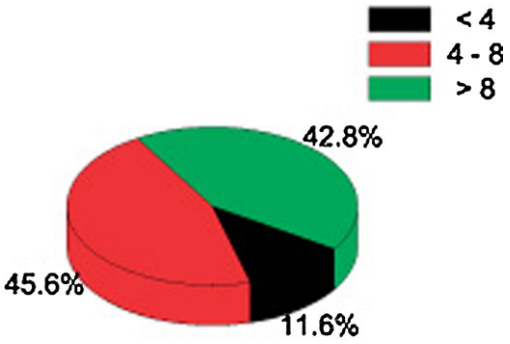

Figure 11 Pie chart illustrating the occurrence of HSS divided into three classes of different durations.

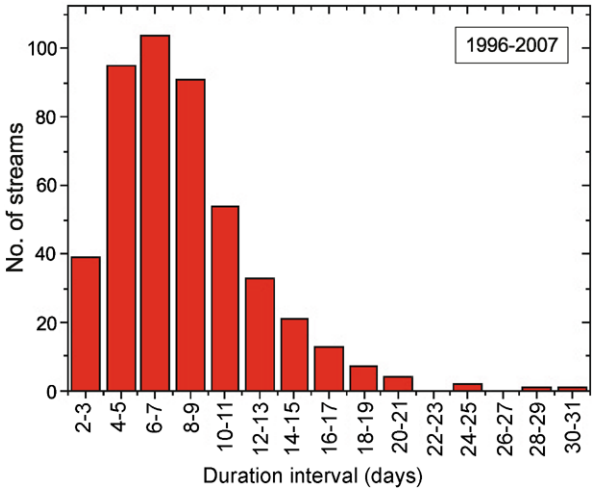

Figure 12 Frequency distribution of HSS duration.

Table 11 Number of streams, classified according to their duration into SD, MD, LD stream, during various condition of solar activity observed during 1996 – 2007.

Phases	SD	MD	LD
Minimum	5	62	42
Increasing	21	54	38
Maximum	15	54	55
Decreasing	13	42	64
Total	54	212	199

SD – short duration, MD – medium duration, LD – long duration.

In Figure 14, we compare the values of plasma/field parameters $\langle V_{max} \rangle$, $\langle N_{max} \rangle$, $\langle T_{max} \rangle$ and $\langle B_{max} \rangle$ with sunspot numbers ⟨SSN⟩ and storm sudden commencements ⟨SSC⟩ during different years of solar cycle 23 (SSN is selected to represent the level of solar activity and SSC to indicate the number of shocks at 1 AU). It can be seen from this figure that $\langle V_{max} \rangle$ is higher during declining activity years while $\langle B_{max} \rangle$, in general, follow the variations in ⟨SSC⟩ and ⟨SSN⟩ (see also King, 1981; Papitashvili, Papitashvili, and King, 2000). However, no definite trend in the variations of $\langle N_{max} \rangle$ and $\langle T_{max} \rangle$ with solar cycle is seen in this figure.

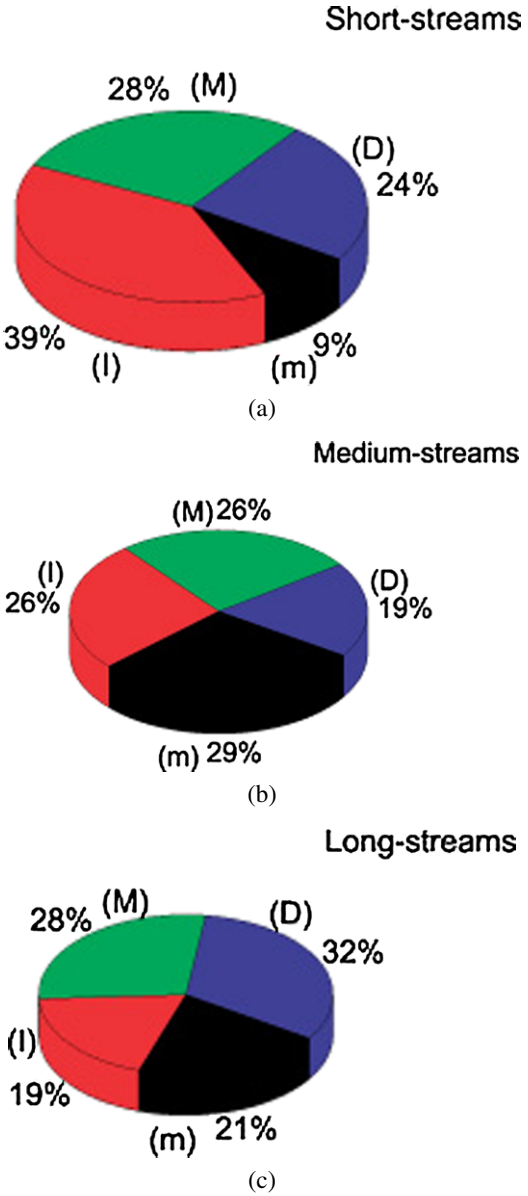

Figure 13 Pie chart illustrating the contribution of HSS of various durations (Short, Medium and Long) during different phases of solar activity in 1996 – 2007.

5. Conclusions

We have prepared a catalog of high-speed streams during solar cycle 23. The solar sources, their duration, *etc*. have been determined. The statistical distribution and plasma/field properties of streams during different years and different phases of solar cycle have been given by classifying the streams on the basis of their sources, speed and duration.

Results of the present analysis are briefly summarized here.

Table 12a Averaged solar-wind parameters during short-duration high-speed stream in various years during 1996 – 2007.

Plasma/field parameters	1996	1997	1998	1999	2000	2001	2002	2003	2004	2005	2006	2007
$\langle V_{max} \rangle$ (km s^{-1})	480	410	492	553	474	582	450	555	562	585	487	0
$\langle N_{max} \rangle$ (cm^{-3})	22	35	22.7	23.3	21.3	29	34.5	21	17.7	27.5	26	0
$\langle T_{max} \rangle$ (10^5K)	1.6	1.4	2.7	3.2	1.7	2.2	1.9	3.7	2.1	1.1	2.1	0
$\langle B_{max} \rangle$ (nT)	9.0	14.0	14.1	15.3	16.0	16.7	15.4	12.0	12.3	16.0	12.2	0

Table 12b Solar-wind parameters during medium-duration high-speed stream in various years during 1996 – 2007.

Plasma/field parameters	1996	1997	1998	1999	2000	2001	2002	2003	2004	2005	2006	2007
$\langle V_{max} \rangle$ (km s^{-1})	552	484	582	565	568	539	547	628	568	603	578	584
$\langle N_{max} \rangle$ (cm^{-3})	25.3	28.7	26	26.1	26.4	36.3	27.1	16.5	14.8	28.3	28.9	26.5
$\langle T_{max} \rangle$ (10^5K)	2.6	2.6	4.3	3.3	3.4	3.5	3.1	3.7	2.8	3.0	3.1	2.8
$\langle B_{max} \rangle$ (nT)	11.5	15.1	17.2	15.6	17.6	18.5	15.7	14.6	12.9	14.4	14.0	11.7

Table 12c Solar-wind parameters during long-duration high-speed stream in various years during 1996 – 2007.

Plasma/field parameters	1996	1997	1998	1999	2000	2001	2002	2003	2004	2005	2006	2007
$\langle V_{max} \rangle$ (km s^{-1})	584	558	590	680	709	643	657	764	643	713	647	662
$\langle N_{max} \rangle$ (cm^{-3})	31.3	35.0	32.3	30.1	33.5	31.1	30.3	25.4	24.2	36.4	26.9	34.4
$\langle T_{max} \rangle$ (10^5K)	3.3	3.0	3.0	5.0	4.3	4.0	4.0	5.5	4.4	4.0	4.0	3.9
$\langle B_{max} \rangle$ (nT)	12.2	15.3	17.8	17.2	23.7	23.5	20.1	19.8	17.9	20.9	14.6	15.5

Table 13 Comparison of averaged peak values of speed, density, temperature and magnetic field due to high-speed streams of different duration, short duration (SD), medium duration (MD) and long duration (LD) observed during 1996 – 2007.

Duration	$\langle V_{max} \rangle$ (km s^{-1})	$\langle N_{max} \rangle$ (cm^{-3})	$\langle T_{max} \rangle$ (10^5K)	$\langle B_{max} \rangle$ (nT)
SD	469 ± 10.54	23.3 ± 1.60	1.9 ± 0.19	12.7 ± 0.60
MD	566 ± 7.11	25.9 ± 0.95	3.2 ± 0.12	14.9 ± 0.39
LD	654 ± 8.59	30.9 ± 0.95	4.0 ± 0.13	18.2 ± 0.67

Of all the HSS identified and categorized into five groups on the basis of their sources, during the period 1996 – 2007, SCH stream is the largest group, while MME group comprises the lowest number of streams.

Division of the whole period of study (1996 – 2007) on the basis of solar activity conditions into low ('minimum'), increasing ('rising'), high ('maximum'), and decreasing ('declining') epochs, each of an equal number of years (three), we observe that SCH streams, in order of decreasing number, occur during low, decreasing, high, and increasing solar ac-

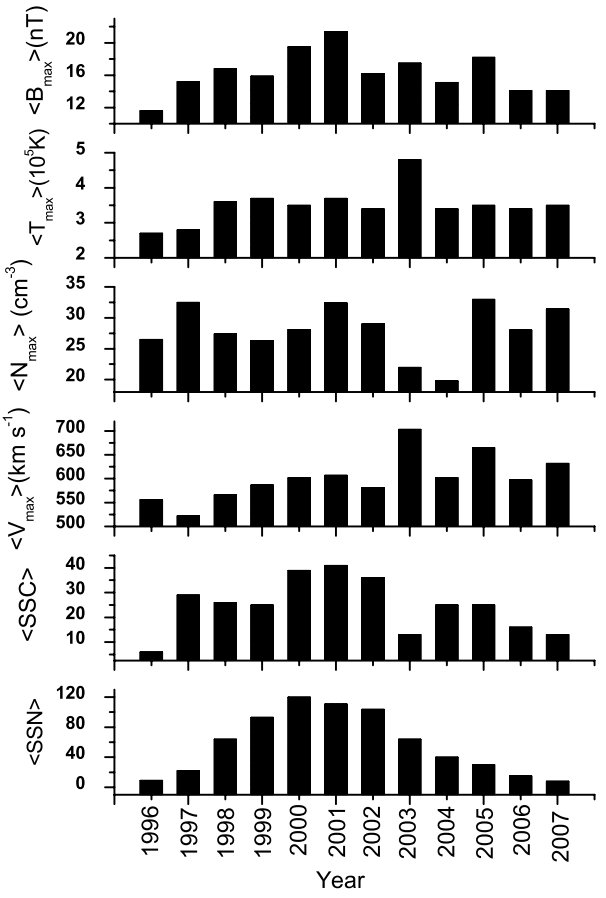

Figure 14 Year-wise comparison of averaged maximum speed, density, temperature and magnetic field in different years from 1996 – 2007 during HSS. The average number of sunspots and SSCs observed in different years are also plotted for comparison.

tivity conditions. The occurrence of MCH streams, during different epochs of solar activity, is almost similar to SCH streams with the majority of them (62%) observed during decreasing and low solar activity, and the rest (38%) observed during increasing and high solar activity conditions. On the other hand, the majority of SME (61%) and CMP (65%) streams occur during increasing and high solar activity conditions. As regards MME streams, most of them (80%) occur during high and increasing activity epochs, and the rest of them (20%) during the decreasing phase.

The averaged parameters $\langle V_{\max} \rangle$, $\langle N_{\max} \rangle$, and $\langle T_{\max} \rangle$ for the whole period (1996 – 2007) of events are, in general, high for interacting streams (MCH, MME, and CMP).

High-speed streams, divided on the basis of speed, irrespective of their source(s), into three speed range 400 – 550 km s^{-1}, 551 – 650 km s^{-1}, and $>$ 650 km s^{-1}, are found to be almost equal in number in each group. The majority (66%) of LS streams (400 – 550 km s^{-1}) occur during increasing and maximum phases of the solar cycle. However, the numbers of MS streams (551 – 650 km s^{-1}) are almost equally divided during minimum, increasing, maximum and decreasing phases of solar cycle. But, of all the HS streams ($>$ 650 km s^{-1}), the highest number occurs during the decreasing phase, while their number is lowest during the increasing phase of solar cycle.

The frequency distribution of HSS divided in a 50 km s^{-1} bin shows that a peak in the distribution lies in 550 – 600 km s^{-1} range, while their numbers are fewer beyond 700 km s^{-1}.

On division of HSS of different durations into three groups, namely, short (< 4 days), medium (4 – 8 days), and long (> 8 days), we observe that streams of duration < 4 days are fewer in number (12%), while the streams of the rest, the other two duration groups, are almost equally divided in number. Out of all Short-streams, there is a clear biasing for them to occur during increasing phase, while a few of them are observed during the maximum phase. However, Medium-streams are almost equally divided during minimum, increasing, maximum and declining phases with a slightly smaller number in the latter phase. As regards the Long-streams, their number is somewhat higher (60%) in maximum and decreasing phases together. The rest occurs in minimum and increasing phases of the solar cycle.

The frequency distribution of streams of different durations divided in a 2-hour bin shows that the maximum number of streams lies in the 6 – 7 hour duration; however, 4 – 5 and 8 – 9 hour duration streams are also quite large in number.

The parameters $\langle V_{\max} \rangle$, $\langle N_{\max} \rangle$, $\langle T_{\max} \rangle$, and $\langle B_{\max} \rangle$ are, comparatively, higher during long-duration streams as compared to streams of short and medium durations.

Yearly averages of peak values in some of the interplanetary parameters from 1996 to 2007 during HSS in different years show that $\langle B_{\max} \rangle$ and $\langle \mathrm{SSC} \rangle$ are highest during a high activity year (2001), while $\langle T_{\max} \rangle$ and $\langle V_{\max} \rangle$ are high during a declining activity year (2003), but $\langle N_{\max} \rangle$ is unusually low during the declining years (2003, 2004).

The results about the identified streams presented and discussed in this work provide further insight in the distribution of their sources, number, speed and duration during different phases of the solar cycle. It is expected that the catalog and statistical results presented in this paper will be of help to stimulate and carry out further studies in solar-terrestrial, space weather and other related areas.

Acknowledgements We are grateful of NASA/NSSDC for making the plasma/field data available through OMNI Web (http://omniweb.gsfc.nasa.gov). Various other catalogs and data available through publications and websites (http://lepmfi.gsfc.nasa.gov; http://cdaw.gsfc.nasa.gov; www.ngdc.noaa.gov; www.srl.caltech.edu/ACE?Wind) useful in this study are also acknowledged with gratitude. We appreciate the generosity of Principal Investigators of various instruments who contributed to these data sets. We also thank the reviewers for their helpful comments.

References

Agrawal, S.P., Ananth, A.G., Bemalkhedkar, M.M., Kargatha, L.V., Rao, U.R.: 1974, *J. Geophys. Res.* **79**, 2269.
Alves, M.V., Echer, E., Gonzalez, W.D.: 2006, *J. Geophys. Res.* **111**, A07S05.
Badruddin: 1997, *Astrophys. Space Sci.* **246**, 171.
Badruddin: 1998, *Planet. Space Sci.* **46**, 1015.
Badruddin: 2002, *Solar Phys.* **209**, 195.
Badruddin: 2006, *J. Astrophys. Astron.* **27**, 455.
Badruddin, Singh, Y.P.: 2009, *Planet. Space Sci.* **57**, 318.
Ballatore, P.: 2002, *J. Geophys. Res.* **107**, 1227.
Borovsky, J.E., Denton, M.H.: 2006, *J. Geophys. Res.* **111**, A07S08.
Bothmer, V., Zhukov, A.: 2006, In: Bothmer, V., Daglis, I. (eds.) *Space Weather: Physics and Effects*, Springer, New York, 31.
Burlaga, L.F.: 1975, *Space Sci. Rev.* **17**, 327.
Burlaga, L.F.: 1991, In: Schwenn, R., Marsch, E. (eds.) *Physics of the Inner Heliosphere II*, Springer, Berlin, 1.
Burlaga, L.F., Behannon, K.W., Klein, L.W.: 1987, *J. Geophys. Res.* **92**, 5725.
Burlaga, L.F., Sittler, E., Mariani, F., Schwenn, R.: 1981, *J. Geophys. Res.* **86**, 6673.
Burns, A.G., Solomon, S.C., Wang, W., Killeen, T.L.: 2007, *J. Atmos. Solar-Terr. Phys.* **69**, 77.

Burton, R.K., McPherron, R.L., Russel, C.T.: 1975, *J. Geophys. Res.* **80**, 4204.
Cane, H.V.: 2000, *Space Sci. Rev.* **93**, 55.
Cane, H.V., Richardson, I.G.: 2003, *J. Geophys. Res.* **108**, 1156.
Cliver, E.W., Drodge, W., Muller-Mellin, R.: 1993, *J. Geophys. Res.* **98**, 15231.
Crooker, N.U.: 2000, *J. Atmos. Solar-Terr. Phys.* **62**, 1071.
Echer, E., Gonzalez, W.D.: 2004, *Geophys. Res. Lett.* **31**, L09808.
Echer, E., Gonzalez, W.D., Tsurutani, B.T., Gonzalez, A.L.C.: 2008, *J. Geophys. Res.* **113**, A05221.
Filisetti, O.B., Lovera, G., Mussino, V., Parisi, M., Villoresi, M.: 1988, *Ann. Geophys.* **6**, 627.
Gold, T.: 1959, *J. Geophys. Res.* **64**, 1665.
Gonzalez, W.D., Joslyn, J.A., Kamide, Y., Kroehl, H.W., Rostoker, G., Tsurutani, B.T., Vasyliunas, V.M.: 1994, *J. Geophys. Res.* **99**, 5771.
Gopalswamy, N.: 2006, *J. Astrophys. Astron.* **27**, 243.
Gopalswamy, N., Akiyama, S., Yashiro, S., Michalek, G., Lepping, R.P.: 2008, *J. Atmos. Solar-Terr. Phys.* **70**, 245.
Gosling, J.T.: 1993, *J. Geophys. Res.* **98**, 18937.
Gosling, J.T.: 1996, *Annu. Rev. Astron. Astrophys.* **34**, 35.
Gosling, J.T., Bame, S.J., McComas, D.J., Phillips, J.L.: 1990, *Geophys. Res. Lett.* **17**, 901.
Gupta, V., Badruddin: 2009, *J. Atmos. Solar-Terr. Phys.* **71**, 885.
Iucci, N., Parisi, M., Storini, M., Villoresi, G.: 1979, *Nuovo Cimento* **2C**, 421.
Iucci, N., Parisi, M., Storini, M., Villoresi, G.: 1984, *Nuovo Cimento* **7C**, 467.
Jian, L.K., Russell, C.T., Luhmann, J.G., Skoug, R.M.: 2006a, *Solar Phys.* **239**, 337.
Jian, L.K., Russell, C.T., Luhmann, J.G., Skoug, R.M.: 2006b, *Solar Phys.* **239**, 393.
Kane, R.P.: 1977, *J. Geophys. Res.* **82**, 561.
Kane, R.P.: 2007, *Adv. Space Res.* **39**, 1890.
King, J.H.: 1981, *J. Geophys. Res.* **86**, 4828.
Klein, L.W., Burlaga, L.F.: 1982, *J. Geophys. Res.* **87**, 613.
Kudela, K.: 2008, *Proc. 30th Int. Cosmic Ray Conf.* **6**, 195.
Kudela, K., Storini, M.: 2005, *J. Atmos. Solar-Terr. Phys.* **67**, 907.
Kudela, K., Storini, M., Hofer, M.Y., Belov, A.: 2000, *Space Sci. Rev.* **93**, 139.
Lepping, R.P., Jones, J.A., Burlaga, L.F.: 1990, *J. Geophys. Res.* **95**, 11957.
Lepping, R.P., Burlaga, L.F., Tsurutani, B.T., Ogilvie, K.W., Lazarus, A.J., Evans, D.S., Klein, L.W.: 1991, *J. Geophys. Res.* **96**, 9425.
Lindblad, B.A., Lundstedt, H.: 1981, *Solar Phys.* **74**, 197.
Lindblad, B.A., Lundstedt, H.: 1983, *Solar Phys.* **88**, 337.
Lindblad, B.A., Lundstedt, H., Larsson, B.: 1989, *Solar Phys.* **120**, 145.
Lockwood, J.A.: 1971, *Space Sci. Rev.* **12**, 658.
Marcz, F.: 1992, *Planet. Space Sci.* **40**, 979.
Maris, O., Maris, G.: 2005, *Adv. Space Res.* **35**, 2129.
Manoharan, P.K., Gopalswamy, N., Yashiro, S., Lara, A., Michalek, G., Howard, R.: 2004, *J. Geophys. Res.* **109**, A06109.
Mavromichalaki, H., Vassilaki, A.: 1998, *Solar Phys.* **183**, 181.
Mavromichalaki, H., Vassilaki, A., Marmatsouri, E.: 1988, *Solar Phys.* **115**, 345.
Mikhailutsa, V.P., Gnevyshev, M.N.: 1985, *Solar Phys.* **98**, 387.
Morley, S.R., Rouillard, A.P., Freeman, M.P.: 2009, *J. Atmos. Solar-Terr. Phys.* **71**, 1073.
Mulligan, T., Russell, C.T.: 2001, *J. Geophys. Res.* **106**, 10581.
Papitashvili, V.O., Papitashvili, N.E., King, J.H.: 2000, *Geophys. Res. Lett.* **27**, 2797.
Parker, E.N.: 1959, *J. Geophys. Res.* **64**, 1675.
Pulkkinen, T.: 2007, *Living Rev. Solar Phys.* **4**, 1.
Rao, U.R.: 1972, *Space Sci. Rev.* **12**, 719.
Richardson, I.G., Cliver, E.W., Cane, H.V.: 2000, *J. Geophys. Res.* **105**, 18203.
Richardson, I.G., Webb, D.F., Zhang, J., Berdichevsky, D.B., Biesecker, D.A., Kasper, J.C., *et al.*: 2006, *J. Geophys. Res.* **111**, A07S09.
Sabbah, I.: 2000, *Can. J. Phys.* **78**, 293.
Schwenn, R.: 2006, *Living Rev. Solar Phys.* **3**, 2.
Schwartz, S.J.: 2006, *Space Sci. Rev.* **124**, 333.
Singh, Y.P., Badruddin: 2007a, *J. Geophys. Res.* **112**, A05101.
Singh, Y.P., Badruddin: 2007b, *J. Geophys. Res.* **112**, A02101.
Srivastava, N., Venkatakrishnan, P.: 2002, *Geophys. Res. Lett.* **29**, 1287.
Shrivastava, P.K., Jaiswal, K.L.: 2003, *Solar Phys.* **214**, 195.
Smith, E.J.: 1983, *Space Sci. Rev.* **34**, 101.
Storini, M., Fillici, A.: 1994, *Nuovo Cimento* **17C**, 697.

Tsurutani, B.T., Gonzalez, W.D.: 1997, In: Tsurutani, B.T., Gonzalez, W.D., Kamide, Y., Arballo, J.K. (eds.) *Magnetic Storms*, *Geophys. Monogr. Ser.* **98**, AGU, Washington, 77.
Tsurutani, B.T., Gonzalez, W.D., Tang, F., Akasofu, S.I., Smith, E.J.: 1988, *J. Geophys. Res.* **93**, 8519.
Tsurutani, B.T., Kamide, Y., Arballo, J.K., Gonzalez, W.D., Lepping, R.P.: 1999, *Phys. Chem. Earth C* **101**, 24.
Turner, N.E., Cramer, W.D., Earles, S.K., Emury, B.A.: 2009, *J. Atmos. Solar-Terr. Phys.* **71**, 1023.
Venkatesan, D., Badruddin: 1990, *Space Sci. Rev.* **52**, 121.
Venkatesan, D., Shukla, A.K., Agrawal, S.P.: 1982, *Solar Phys.* **15**, 247.
Xie, H., Gopalswamy, N., Manoharan, P.K., Lara, A., Yashiro, S., Lepri, S.: 2006, *J. Geophys. Res.* **111**, A01103.
Zhang, G., Burlaga, L.F.: 1988, *J. Geophys. Res.* **93**, 2511.
Zhang, J., Richardson, I.G., Webb, D.F.: 2008, *J. Geophys. Res.* **113**, A00A12.
Zhang, J., Poomvises, W., Richardson, I.G.: 2008, *Geophys. Res. Lett.* **35**, L02109.
Zhang, J., Liemohn, M.W., Kozyra, J.U., Lynch, B.J., Zurbuchen, T.H.: 2004, *J. Geophys. Res.* **109**, A09101.
Zhang, J., Richardson, I.G., Webb, D.F., Gopalswamy, N., Huttunen, E., Kasper, J.C., *et al.*: 2007, *J. Geophys. Res.* **112**, A10102.